

# On the potential of probing the neutron star composition in accreting X-ray binaries

Kaiser Arf and Kai Schwenzer

*Istanbul University, Science Faculty, Department of Astronomy and Space Sciences, Beyazit, 34119, Istanbul, Turkey*

Transiently accreting Low Mass X-Ray Binaries have the potential to probe the core composition of their neutron stars via deep crustal heating caused by nuclear reactions. We statistically assess this deep crustal heating scenario, taking into account the various microphysical and astrophysical uncertainties. We find that despite the sizable uncertainties there is the chance to discriminate different compositional scenarios. Several observed sources statistically challenge a minimal hadronic matter composition, where cooling proceeds exclusively via slow modified Urca reactions. Considering here two exemplary extended uniform compositions, namely ultra-dense hadronic matter with direct Urca emission and ungapped quark matter, we find that they are even within uncertainties distinguishable. We show that although exotic forms of matter are generally only expected in an inner core, which could in principle have any size, sufficiently large astrophysical data sets nonetheless have the potential to statistically discriminate compositional scenarios, in particular when further mass measurements become available.

## I. INTRODUCTION

The observed Low Mass X-ray Binaries (LMXBs) [1] are thought to be neutron stars [2, 3] in the later stage of their recycling process [4], accreting from a low mass companion via Roche lobe overflow [5]. Many of them are transiently accreting systems and show strong, and typically short, outbursts followed by longer periods of quiescence, where the luminosity is significantly smaller. While both the peak luminosity and the quiescence period can vary between outbursts as well as between different sources, over long time intervals these sources are by energy conservation expected to reach a steady state where the accretion heating balances the cooling due to both bulk neutrino and surface photon emission [6–8].

The interior of the star is strongly thermally insulated from its surface by the outermost layers of the crust where both the density and the thermal conductivity decrease dramatically, so that nearly all of the gravitational potential energy deposited during outburst is quickly radiated from the surface layer, having a small heat capacity [9–11]. Yet, over time material is buried under a growing layer of subsequently accreted material and eventually transforms to successively heavier nuclei as the density and pressure on it increases. It has been shown that the nuclear energy from pycno-nuclear reactions deep in the crust, fusing lighter into heavier nuclei, can produce a significant amount of heat [12–16]. This deep crustal heating [17] directly heats the core of the star and can therefore inform us about the cooling process(es) [6], which strongly depend on the composition. This long term thermal state should be reflected after a sufficiently long time in quiescence when the thermal profile in the crust relaxed back to its steady state profile, while the average heating power can be obtained from the luminosities in and time intervals between outbursts [8].

Since the long-term steady state of the system is completely determined by energy conservation, this provides for a given star composition a direct analytic relation between the observable thermal quiescence luminosity and

average accretion rate, that can be compared to astrophysical data. However, this relation involves many microscopic and macroscopic parameters some of which involve significant uncertainties. The largest uncertainty stems from the surface composition [10, 18] and we consider the two extreme cases of a fully catalyzed [19] and a fully accreted envelope [13] separately. We estimate and take into account the other uncertainties and perform a statistical analysis to determine how compatible a given compositional scenario is with the astrophysical data for a given source. We quantify this by corresponding probabilities and find that even taking into account these various uncertainties some of these probabilities are remarkably small, so that the corresponding compositional scenario can be statistically ruled out. Taking into account that the effect of superfluidity is still rather uncertain, we use the minimal cooling of  $npe\mu$ -matter with modified Urca neutrino processes [20] as a baseline, and find that there are several sources that challenge this minimal scenario. This requires enhanced cooling mechanisms and we consider here the extreme case of direct Urca processes in both hadronic [21] and quark matter [22].

## II. LONG-TERM THERMAL STEADY STATE

In compact stars the inner energy (and its change) is tiny compared to their total energy and therefore the thermal evolution can be considered within the background structure of a static cold star [23, 24]. The metric of a spherically symmetric mass configuration is described by the Schwarzschild metric

$$ds^2 = e^{2\phi(r)} dt^2 - \left(1 - \frac{2Gm(r)}{r}\right)^{-1} dr^2 - r^2 d\Omega^2$$

in terms of two metric functions:  $m(r)$  the mass within radius  $r$ , and  $\phi(r)$  which is in the non-relativistic limit related to the Newtonian gravitational potential. A static

compact star is then completely described by the density distribution and composition within the star and is obtained from a solution of the TOV equation [25, 26]. At the surface and outside of the star, where  $m(r)$  is constant  $m(r \geq R) = M$ , the curvature is completely described by the potential  $\phi(r \geq R) = \frac{1}{2} \log(1 - \frac{2GM}{r})$ .

In the most outer part of the crust of a neutron star the density and correspondingly also the thermal conductivity drops dramatically, effectively presenting an insulating layer. The temperature  $T_b$  at the inner boundary of this insulating layer can therefore strongly differ from temperature the  $T_s$  at the surface [27], which due to the small thickness of the insulating layer is roughly obtained at the radius  $R$ . The global thermal evolution of a accreting star is determined by energy conservation and takes the form [28, 29]:

$$C_V(T_b) \frac{dT_b}{dt} = P_h^\infty - L_\nu^\infty(T_b) - L_\gamma^\infty(T_s) \quad (1)$$

where  $P_h^\infty$ ,  $L_\nu^\infty$  and  $L_\gamma^\infty$  are the heating power, the neutrino luminosity from the bulk and the surface photon luminosity, all considered at a reference frame at infinity.

When averaging over many outburst/quiescence cycles, the star should eventually reach a steady-state [6, 29, 30] where the temperature does not change anymore and correspondingly the heating roughly balances the cooling

$$P_h^\infty \approx L_\nu^\infty + L_\gamma^\infty \quad (2)$$

Here we consider the strong heating due to the accretion, neglecting other potential heating mechanisms, e.g. rotochemical heating [31] or dissipative damping of unstable oscillation modes [32, 33]. In particular r-mode heating could be sizable if the r-mode amplitude is large. However, by now there are strict bounds on the r-mode amplitude in millisecond pulsars [34] that are more than an order of magnitude below those from LMXBs and since the r-mode saturation mechanism should at most be weakly temperature dependent also r-mode heating should indeed be minor in LMXBs. LMXBs, being very old, have small dipole magnetic fields so that their potential impact on the heating can likewise be neglected.

While the surface heating from the accretion during outburst is, owing to the insulating layer and the small heat capacity of the outermost part of the crust, nearly immediately radiated off, only the heating due to pycnonuclear reactions deep in the crust can actually heat the interior. This deep crustal heating is determined by the average amount of energy per baryon  $Q$  deposited deep in the crust [14, 16, 35], and the heating power as seen from infinity reads [36]

$$P_h^\infty \equiv \frac{Q}{m_N} \langle \dot{M} \rangle e^{\phi(R)} \quad (3)$$

where  $e^{\phi(R)}$  is the spatial component of the Schwarzschild metric at the surface of the star,  $m_N$  the nucleon mass and  $\langle \dot{M} \rangle$  is the average mass accretion rate.

The neutrino luminosity depends strongly on the core composition and the temperature. The core temperature of a neutron star is not directly observable but sufficiently long after outburst the crust, which was pushed out of equilibrium by the accretion heating, relaxes back to the quasi-equilibrium thermal profile and there is a unique dependence between the temperature  $T_b$  below and the surface temperature  $T_s$  above the insulating layer that takes the form [19]

$$\frac{T_s^4}{g_s} = f(T_b) \approx c T_b^{4\gamma} \quad (4)$$

where  $g_s$  is the surface gravitational field  $g_s = e^{-\phi(R)} GM/R^2$  in terms of the temporal metric factor  $e^\phi$ . The precise function  $f$  in eq. (4) is obtained by solving the heat-conduction throughout the insulating layer and over the relevant temperature range it is to good accuracy described by a simple power law form [19, 37]. The precise relation, described by the parameters  $c$  and  $\gamma$ , depends on the composition of the crust.

Owing mainly to the heat transport by light and merely electromagnetically interacting electrons, the thermal conductivity below the insulating layer is very large. Thorne [23, 24] and Glen [28] studied thermal transport in the curved spacetime inside of a neutron star and found that owing to energy conservation even in the limit of an infinitely large thermal conductivity the star is not isothermal, but rather the total particle energy (kinetic and potential) is constant resulting in  $T(r) e^{\phi(r)} = \text{const}$ . Using this relation, the temperature anywhere inside the star is given in terms of the temperature  $T_b$  at the inner boundary of the insulating layer, which is approximately located at the radius  $R$  of the star, via

$$T(r) = T_b \frac{e^{\phi(R)}}{e^{\phi(r)}} \quad (5)$$

The local neutrino emission due to a process  $i$  is described by the neutrino emissivity  $\epsilon_i(r)$  which in general has the following dependence on the local temperature [38]

$$\epsilon_i(r) = \tilde{\epsilon}_i(n(r), x_s(n(r)), \dots) T(r)^{\theta_i} \lambda(r)^{\Theta_i} \quad (6)$$

where  $\theta_i$  denotes the power law exponent characterizing the mechanism,  $\tilde{\epsilon}_i$  is a temperature-independent pre-factor and the last factor describes logarithmic non-Fermi liquid corrections in certain phases of dense quark matter [39], which we will neglect in this work (i.e. here  $\Theta = 0$ ). The pre-factor generally depends on other local quantities like the overall baryon density  $n$  as well as particle fractions  $x_s$  of the different species  $s$ , which in equilibrium are functions of the baryon density. Taking into account that a neutron star is a strongly degenerate system

where  $T/\mu \lesssim 10^{-4}$  in particular the exponent  $\theta$ , ranging from slow processes ( $\theta = 8$ ) to fast processes ( $\theta = 6$ ), has a dramatic impact on the cooling [40]. It is determined by qualitative aspects of the low energy degrees of freedom and their interactions and alters the luminosity by many orders of magnitude for different phases of dense matter, potentially allowing us a clear discrimination despite the various micro- and macro-physical uncertainties.

The total luminosity at infinity is then obtained by integrating the neutrino emissivity over the entire star, taking into account the spatial volume factor  $\sqrt{\det(g_{ij})} = (1 - 2Gm(r)/r)^{-1/2}$  and the appropriate red-shifting,

$$L_{\nu,i}^{\infty} = \int d^3r \sqrt{\det(g_{ij})} \quad (7)$$

$$\times \tilde{\epsilon}_i(n(r), x_s(n(r)), \dots) \left( T_b \frac{e^{\phi(R)}}{e^{\phi(r)}} \right)^{\theta_i} e^{2\phi(r)}$$

This expression can be written in the form

$$L_{\nu,i}^{\infty} = \frac{M}{n_0 m_N} \hat{\epsilon}_i(n_0, x_s(n_0), \dots) T_b^{\theta_i} \tilde{L}_i \quad (8)$$

in terms of the luminosity of a hypothetical uniform star of mass  $M$  in the absence of gravity—i.e. literally a dramatically scaled up atomic nucleus, with matter at saturation density  $n_0$  [41], having a Euclidean volume  $V = M/(n_0 m_N)$ , where  $m_N$  is the nucleon mass—and a dimensionless constant factor  $\tilde{L}_i$  that takes into account all effects of gravity, i.e. the detailed spacetime curvature, density distribution and local composition within the star

$$\tilde{L}_i \equiv \frac{4\pi n_0 m_N}{M} \int_0^R dr r^2 \left( 1 - \frac{2Gm(r)}{r} \right)^{-1/2} \quad (9)$$

$$\times \frac{\hat{\epsilon}_i(n(r), x_s(n(r)), \dots)}{\hat{\epsilon}_i(n_0, x_s(n_0), \dots)} \left( \frac{e^{\phi(R)}}{e^{\phi(r)}} \right)^{\theta_i} e^{2\phi(r)}$$

This dimensionless constant absorbs the entire dependence on the poorly known equation of state. All factors in the emissivity ratio that are not radius-dependent cancel in eq. (9) and this constant can be numerically computed for different star configurations based on different equations of state. Interestingly, we find that  $\tilde{L}$  is close to 1 for a  $1.4 M_{\odot}$  star with an APR equation of state [42] cooling via Urca processes [20, 43]—i.e. the total effect of gravity is actually not that big, and this only strongly changes as one goes close to the maximum mass configuration.

The neutrino luminosity for known emission mechanisms is strongly temperature-dependent ( $\theta_i \gtrsim 6$ ) and therefore it largely dominates the photon surface emission  $L_{\gamma} \sim T_s^4$  sufficiently above the temperature  $T_e$ , where they are of equal size, and approximately alone balances the heating in eq. (2), i.e.  $L_{\nu,i}^{\infty}(T_b) \approx L_h^{\infty}$ , which determines the steady state temperature below the insulating layer. Using eq. (4) this can be related to the

surface temperature outside of the insulating layer, and using the Stefan-Boltzmann law finally to the effective photon luminosity in quiescence red-shifted to infinity, which takes for  $T$  sufficiently above  $T_e$  the explicit analytic form

$$L_{\gamma}^{\infty} = 4\pi\sigma R^2 T_s^4 e^{2\phi(R)} = 4\pi\sigma R^2 g_s c T_b^{4\gamma} e^{2\phi(R)} \quad (10)$$

$$\approx 4\pi\sigma c G M^{1 - \frac{4\gamma}{\theta_i}} e^{(1 + \frac{4\gamma}{\theta_i})\phi(R)} \left( \frac{n_0 Q \langle \dot{M} \rangle}{\hat{\epsilon}_i(n_0, x_s(n_0), \dots) \tilde{L}_i} \right)^{\frac{4\gamma}{\theta_i}}$$

where  $\sigma$  is the Stefan-Boltzmann constant. Note that in eq. (10)  $\theta_i > 4$  and  $\gamma < 1$  so that this result is fortunately rather insensitive to the various parameters describing the process, which can have sizable uncertainties. In particular the leading power-law dependence on the radius cancels out and leaves only the indirect dependence via the metric factor. Yet, eq. (10) sensitively depends on the power law exponents  $\theta_i$  and  $\gamma$  characterizing the neutrino emission in qualitatively different forms of dense matter in the interior of the star, as well as the crust composition, respectively.

Averaging over several outbursts the average accretion rate in turn can be obtained from the average outburst luminosity and the average recurrence time, taking into account that the gravitational potential energy of the accreted mass is deposited as heat on the surface and (owing to the small heat capacity of the envelope) immediately radiated off during the accretion phase. The accretion should happen dominantly at the magnetic poles of the star creating hot spots. Yet the accreted material and the heat is eventually distributed over the surface of the star. As long as the surface luminosity significantly exceeds the luminosity of the hot spot (which is typically the case due to its small size), this complication can be neglected.

If in contrast the temperature is sufficiently below  $T_e$  the photon luminosity strongly dominates neutrino cooling so that the photon luminosity fulfills the simpler relation

$$L_{\gamma}^{\infty} \approx P_h^{\infty} = \frac{Q}{m_N} \langle \dot{M} \rangle e^{\phi(R)}$$

Correspondingly the deep crustal heating scenario cannot probe the interior composition of the star in cold sources and the detailed transition point  $T_e$  depends on the emission mechanism. In between these two regimes there is a (typically narrow) transition region, where both cooling mechanisms are relevant, that can be studied by a numerical solution of eq. (2). Here we will concentrate on the asymptotic regimes, since only the explicit analytic expressions allow us a systematic assessment of the various uncertainties involved in the analysis.

Finally in a star with fast (direct Urca) cooling  $L_{\nu f}^{\infty}$  in an inner core of mass  $M_c$  and slow (modified Urca) cooling  $L_{\nu f}^{\infty}$  in the surrounding mantle, neglecting surface

emission, the steady state equation can be written in the terms of the mass fraction

$$P_h^\infty \approx \left(1 - \frac{M_c}{M}\right) L_{\nu s}^\infty + \frac{M_c}{M} L_{\nu f}^\infty \quad (11)$$

which gives for the required mass fraction at a given temperature  $T_b$

$$\frac{M_c}{M} \approx \frac{P_h^\infty - L_{\nu s}^\infty(T_b)}{L_{\nu f}^\infty(T_b) - L_{\nu s}^\infty(T_b)} \quad (12)$$

### III. STAR COMPOSITION

#### 1. Neutron star envelope $T_b - T_s$ relation

The composition of the envelope of the neutron star has a strong impact on the insulation and its composition is altered by the accreted matter [3]. The envelope composition thereby introduces a significant uncertainty when trying to determine the interior composition of the star from astrophysical data. Here we consider two extreme cases: a pure iron (non-accreted) envelope [19] and a light element (fully accreted) envelope [13]. The envelopes of actual accreting sources should be somewhere in between these two limits, but we refrain from considering such intermediate cases since they depend on model assumptions on the composition of the crust. The  $T_b - T_s$  relation for a non-accreted iron envelope was given in [19], were a good fit to numerical heat transport simulations throughout the heat blanket takes the form

$$T_{s6} = \left(0.1288^{-\frac{1}{0.455}} g_{s14}\right)^{\frac{1}{4}} T_{b9}^{\frac{1}{1.82}} \quad (13)$$

where  $T_{b9}$  is the normalized boundary temperature  $T_{b9} = T_b/10^9$  K,  $T_{s6}$  is the normalized surface temperature  $T_{s6} = T_s/10^6$  K and  $g_{s14} \equiv g_s/10^{14}$  cm/s<sup>2</sup> is the normalized surface gravitational acceleration of neutron stars. Similarly the surface temperature relation for a fully accreted envelope was been given for boundary temperatures  $T_b \leq 10^8$  K as [13]

$$T_{s6} = \left(18.1^{2.42} g_{s14}\right)^{\frac{1}{4}} T_{b9}^{\frac{2.42}{4}} \quad (14)$$

#### 2. Basic neutrino emission processes

The local, microscopic quantity that can distinguish different compositions in the neutron star interior is the neutrino emissivity [40], dominating the heat loss in sufficiently hot sources. In ungapped, uniform phases of matter it is generally Urca processes that dominate the neutrino emission. The simplest composition is hadronic  $npe\mu$ -matter where direct Urca processes are forbidden by momentum conservation at sufficiently low density. In

this case only modified processes [20] are possible where another collision with a bystander particle via the strong interaction is necessary to provide the required momentum

$$(n, p) + p + e^- \longrightarrow (n, p) + n + \nu_e \quad (15)$$

$$(n, p) + n \longrightarrow (n, p) + p + e^- + \bar{\nu}_e \quad (16)$$

and these processes are correspondingly strongly suppressed. The star is in chemical equilibrium with respect to these processes and moreover has to be locally charge neutral. The expression for the modified URCA neutrino emissivity in the pion-exchange approximation valid for the long-range part of the nuclear force was derived in [20] and an approximation for its short-range component was considered. The long range part is obtained from a chiral expansion and takes the simple form (in natural units  $\hbar = c = 1$ )

$$\epsilon_{mU} = \frac{11513}{60480} \frac{G_F^2 g_A^2}{2\pi} \alpha_{\text{Urca}} \beta_{\text{Urca}} \left(\frac{f}{m_\pi}\right)^4 (m_n^*)^3 m_p^* p_{Fe} (k_B T)^8 \quad (17)$$

from which one can read off  $\hat{\epsilon}_{mU}$  and  $\theta_{mU} = 8$ , which characterizes a *slow* process. Here  $G_F$  is the Fermi coupling,  $g_A$  is the axial coupling and  $m^* = p_F/v_F$  are effective masses. The parameter  $\alpha_{\text{Urca}}$  is a correction factor including both a mild non-power-law density dependence as well as off-shell effects, that were neglected in [20], but turned out to be sizable and were taken into account in [44]. The contribution from short-range correlations is due to the present impossibility to solve strongly coupled QCD at high density [45] still rather model dependent and in particular could also have a somewhat different density dependence than eq. (17). To take into account these uncertainties without having to make particular assumptions on the detailed form of the emissivity, we added another correction factor  $\beta_{\text{Urca}}$  in eq. (17) that reflects this uncertainty and which will be chosen below in order that the expected physical curve lies within the corresponding enlarged error band. The arising electron Fermi momentum is given in terms of the baryon density and the electron fraction via  $\mu_e \approx p_{Fe} = (3\pi^2 x_e)^{\frac{1}{3}} n^{\frac{1}{3}}$ . There are even slower processes (like bremsstrahlung), but since modified Urca will be there as long as the nucleons are not entirely paired these are typically negligible.

At sufficiently high density where the proton fractions exceeds a critical value  $x_{pc}$  somewhere between 11 – 15%, depending on the muon concentration, the nucleonic direct Urca channel

$$p + e^- \longrightarrow n + \nu_e \quad (18)$$

$$n \longrightarrow p + e^- + \bar{\nu}_e \quad (19)$$

gradually opens up over a rather narrow density interval where the Urca emissivity ramps up by many orders

of magnitude [44] (while the corresponding direct muon process opens only at even higher proton fractions and is therefore mostly negligible). This transition can approximately be described by a step function  $\Theta$ , and its emissivity is given by [21]

$$\epsilon_{\text{dU}} = \frac{457\pi}{10080} G_F^2 \cos^2 \theta_c (1 + 3g_A^2) m_n^* m_p^* \mu_e (k_B T)^6 \Theta \quad (20)$$

which represents a *fast* process with  $\theta_{\text{dU}} = 6$ . Taking into account that in neutron stars  $T_b/p_F = O(10^{-4})$ , the direct rate is parametrically enhanced by many orders of magnitude. Yet, relying merely on weak interactions this process is less uncertain than the modified version. If the central density is above the critical density for direct Urca reactions there will be a core within the neutron star that emits with the much higher emissivity eq. (20), whereas the rest of the star emits with the much lower emissivity eq. (17) and will be negligible if the core is sufficiently large.

Owing to the asymptotic freedom of QCD, at high density deconfined 3-flavor quark matter ( $u, d, s$ ) could exist in the star. In this case the analogous Urca processes at the quark level are relevant

$$u + e \longrightarrow d + \nu_e \quad (21)$$

$$d \longrightarrow u + e + \bar{\nu}_e \quad (22)$$

The neutrino emissivity for quark Urca processes identically vanishes for massless, non-interacting fermions [22, 46]. According to chiral symmetry restoration in deconfined quark matter the quark masses are expected to be small, but since the interactions are still sizable, the leading correction stems from radiative corrections to the quark self-energy and the emissivity gives to leading order in resummed perturbation theory [22],

$$\epsilon_{\text{qU}} = \frac{914}{315} G_F^2 \cos^2 \theta_c \alpha_s p_{Fd} p_{Fu} p_{Fe} (k_B T)^6 \quad (23)$$

which is likewise a fast process  $\theta_{\text{qU}} = 6$ , but since the direct Urca rate vanishes for free ultra-relativistic particles and quarks are much closer to that limit than massive hadrons the prefactor of the quark emissivity is parametrically smaller than that of the hadronic process. The analogous neutrino processes involving a strange quark are suppressed in the Cabbibo angle  $\theta_c$  and can to leading order be neglected. Taking into account that symmetric 3-flavor quark matter is automatically charge neutral, the electron Fermi momentum is determined by the mass imbalance and when neglecting the masses of the light quarks effectively by the strange quark mass  $p_{Fe} \approx m_s^2 / (4p_{Fq})$ . Since eq. (23) is a result of resummed perturbation theory it could receive sizable corrections in the still rather strongly coupled regime realized in neutron star matter. This dependence on non-perturbative effects is also reflected in the size of the strong coupling

$\alpha_s$  which is already rather uncertain in the vacuum [47], and even more so in dense matter. Instead of introducing another multiplicative parameter that takes into account that non-perturbative effects will change this result, we rather consider the strong coupling in eq. (23) as an effective parameter and the uncertainty range we use for it below will include the combined estimated impact of non-perturbative effects on the neutrino emission.

Interacting quark matter can also be in a color superconducting state [48]. Even in this case there are typically ungapped quark flavors which dominate the neutrino emission, and sufficiently below the critical temperature of the superconductor the emissivity is in uniform phases effectively simply given by eq. (23) times a suppression factor reflecting the reduced number of ungapped flavors. The exception is the CFL phase [48] where all quark flavors pair in a particular symmetric way. As mentioned, if the quarks interact via unscreened gluons, which is the case in certain quark phases, the emissivity involves a non-Fermi liquid enhancement [39] which introduces an additional logarithmic temperature dependence that we will neglect in this work.

The fact that the simplest compositional scenario, namely hadronic  $npe\mu$ -matter, can feature both very slow as well as the fastest known processes, and that, depending on the equation of state, the fast component can be realized in a core of varying size, shows that it is inherently hard to observationally confirm other compositional scenarios. Nonetheless there is a unique equation of state in nature and therefore a very narrow mass range where the direct Urca channel opens up. Therefore, with sufficient statistics and additional mass observations such a discrimination could be possible if all the uncertainties in the analysis can be accounted for.

#### IV. ESTIMATING MICROPHYSICAL AND ASTROPHYSICAL UNCERTAINTIES

To obtain robust results on whether a particular compositional scenario can be realized in observed astrophysical sources, requires an assessment of the many uncertainties in the process. The above expressions eqs. (10), (13), (14), (17), (20) and (23) depend both on bulk properties of astrophysical sources as well as the microscopic uncertainties related to the underlying transport and emission processes. In the following we estimate the uncertainties of the various input parameters and determine their impact on the relation eq. (10) between the quiescence thermal luminosity and the mass accretion rate. In many cases it is surely impossible to rigorously determine the uncertainty of poorly known astrophysical or microphysical input parameters to a well defined significance. In these cases we estimate a *conservative maximum interval* that these parameters should, according to what we know about the underlying physics, lie in. For a conservative analysis we consider this “maximum interval” as a  $2\sigma$  interval of a Gaussian probability

distribution, taking into account that what is currently conceivable could be with a small probability too limited or biased, and might have to be revised as new data or theoretical insight becomes available. In the following we discuss all arising parameters and estimate their ranges, and the resulting  $1\sigma$  intervals are also compiled in table I individually:

**$M$ :** For most considered astrophysical sources the neutron star mass is not known, so that we have to estimate a mass range for these sources. Theoretically the mass could be very low but it is limited by the birth process in a core collapse supernova and our minimum bound stems from the smallest observed neutron star mass,  $M_c = (1.174 \pm 0.004) M_\odot$  obtained for the companion of the pulsar J0453+1559 [49]. While these sources in double neutron star systems likely never accreted, the sources in LMXBs studied here have an accretion history and should likely be significantly heavier, but since it is hard to estimate by how much we use  $M_{\min} = 1.2 M_\odot$  as a conservative lower bound for LMXBs as well. The maximum mass is harder to estimate, but has to be larger than the masses of observed sources slightly in excess of  $2M_\odot$  [50], including in particular very precise measurements from Shapiro delay [51, 52]. A more recent study [53] found an even larger, but somewhat more uncertain mass  $M = (2.35 \pm 0.17) M_\odot$ . Actual upper bounds can be obtained from neutron star merger giving a mass bound  $M_{\text{TOV}} \lesssim (2.16 \pm 0.17) M_\odot$  [54, 55]. The masses of rotating stars can be larger than the static TOV mass by  $M_{\text{rot}} \lesssim (1.20 \pm 0.05) M_{\text{TOV}}$  [54]. While for sources spinning with presently observed spin frequencies the effect should be smaller, an exotic composition might increase these values to some extent. When considering these maximum masses one in particular has to take into account that a theoretical equilibrium configuration with maximum TOV or rotational mass (which will collapse at the smallest disturbance) is not a realistic possibility for a source that is billions of years old and regularly suffers cataclysmic events—like the accretion of huge amounts of matter (up to nearly the mass of the moon in a short time interval on an object the size of a city) or thermonuclear explosions covering the entire surface of the star. Based on all these constraints we choose a conservative upper bound of  $2.5 M_\odot$ , resulting in the  $1\sigma$  range in table I.

**$R$ :** The radius is mainly determined by observations of the thermal x-ray emission from the star’s surface [56, 57]. Generally these studies have large uncertainties in mass-radius space, but taking into account that radii from TOV solutions are generically rather insensitive over a wide range of masses, the radius can be constrained with sufficient statistics. The improved accuracy of NICER allowed to obtain

precise values for individual sources. The most precise values stem from the  $1.4 M_\odot$  star J0030+0451 [58] and the  $\approx 2.1 M_\odot$  star J0740+6620 [59] which when combined with other constraints yield expected radii  $(12.45 \pm 0.65)$  km for  $1.4 M_\odot$  and  $(12.35 \pm 0.75)$  km for  $\approx 2.1 M_\odot$ . Even heavier sources can be expected to be more compact, in particular if they have an exotic composition [60]. Based on all these studies we estimate the maximum conservative interval for the radii of neutron stars in the above mass range between 10 km and 13.7 km. This interval also includes the smaller impact of the non-catalyzed crust on the equation of state and in turn on the structure of lighter stars [61].

**$Q_B$ :** Describing the deep crustal heating requires simulations of the nuclear composition and of the various different reaction channels as the accreted material is processed to heavier elements via electron capture, neutron emission and in particular pycnonuclear reactions [12, 14, 15]. The pycno-nuclear fusion reactions require tunneling and can only happen at sufficiently high density. The total heating can be described by the average heat energy per baryon  $Q_B$  deposited within all these reactions deep in the crust. Although the simulations are complicated and the detailed reaction path can sensitively vary, the quantity  $Q_B$  is fortunately less sensitive since eventually “the entire nuclear fuel is burned” irrespective of the detailed reactions, and heats the star unless part of it is lost via neutrino processes that are part of the reaction path. To estimate these effects [15] considered two extreme cases at which pycno-nuclear reactions start to operate ( $A_i = 56$  vs.  $A_i = 106$ ) as well as the extreme cases of maximum neutrino losses and the complete blocking of the neutrino emission. This way an interval  $1.16 \text{ MeV} \lesssim Q_B \lesssim 1.93 \text{ MeV}$  was obtained. Using a multi-component liquid drop model slightly larger values were found in [62]. More recently the heating was considered in a density functional theory, considering nuclear shell effects but neglecting neutrino losses [16], giving the narrow range  $1.5 \text{ MeV} \lesssim Q_B \lesssim 1.7 \text{ MeV}$ . In view of the still slightly differing results obtained in different approximations we consider a conservative maximum interval of  $1.2 \text{ MeV} \lesssim Q_B \lesssim 2 \text{ MeV}$ , giving the  $1\sigma$  uncertainty in table I.

**$\tilde{L}_i$ :** As discussed in section II this parameter effectively takes into account the effect of gravity on the neutrino emission, and describes its deviation in a realistic star compared to a large uniform atomic nucleus. It depends both on the equation of state and the particular stellar configuration (characterized by its mass). Here we consider an APR equation of state [42] for hadronic matter and a bag model for quark matter and consider different stel-

lar configurations to numerically compute the constants eq. (9) for the considered Urca processes. We find that, aside for configurations close to the mass limit, the impact of gravity is actually quite modest, while, as discussed, configurations close to the mass limit are not realistic for these sources anyway. Correspondingly considering APR configurations between  $1.2 M_\odot$  and  $2 M_\odot$  (while the maximum mass limit of the APR is already at  $2.2 M_\odot$ ) yields e.g. for modified Urca reactions a range  $1.16 \lesssim \tilde{L}_{\text{mU}} \lesssim 1.90$  and we double this error range in order to take into account the uncertainties due to the equation of state.

$\alpha_{\text{Urca}}$ : The modified Urca amplitude has a non-power law dependence that was originally absorbed in this factor in [20] which amounted to a small correction close to one. More recently in [44] also off-shell effects, that were ignored in the originally derivation [20], were included in this factor and they result in a sizable enhancement of the rate and according to the conventions of [44] also include the gradual opening of the direct Urca channel [63]. In this work we consider the direct Urca channel separately and in order to only take into account uncertainties due to the complicated density dependence of the modified Urca rate we consider the behavior sufficiently away from threshold, giving a conservative maximum interval  $5 \leq \alpha_{\text{Urca}} \leq 13$ .

$\beta_{\text{Urca}}$ : Via this factor (called  $R_{\text{Urca}}$  in [20]) that multiplies the (analytic) result for the modified Urca rate due to long-range pion exchange [20], we take into account the effect of repulsive short-range correlations. As a guide we considered the (model-dependent) results obtained in the same article within an operator product expansion (OPE), which increase the emissivity, and we further increased the uncertainty range assuming a conservative maximum interval of  $2/3 \lesssim \beta_{\text{Urca}} \lesssim 2$ .

$\alpha_s$ : Since the Urca rate vanishes for free, ultra-relativistic particles [22, 46], neutrino emission in dense quark matter requires strong interactions to open up phase space. As discussed, we consider  $\alpha_s$  as an effective parameter that takes into account the effect of the non-perturbative strong dynamics. There are no controlled non-perturbative QCD computations at large baryon density so far [45]. While the coupling becomes small in the asymptotically free regime at large scales, experimental studies and vacuum computations show that at energies of a few hundred MeV, corresponding to the densities in neutron stars, the coupling is still quite large and not so far from its infrared value  $\alpha_s \approx 1 - 3$  [47]. In order to consider the impact of other non-perturbative effects we consider the upper value also as the upper bound of our conservative interval for the effective parameter  $\alpha_s$  even in dense

quark matter. Charge screening should to some extent weaken the interaction, but the experimental value for the running coupling from  $\tau$ -decay into hadrons takes already a value  $\alpha_s(m_\tau^2) \approx 0.3$  at the much larger scale  $m_\tau \approx 1.8 \text{ GeV}$  [64]. Effects due to charge screening and their impact on the quark self-energy corrections, that affect their dispersion relations, only become relevant at the significantly lower quark Fermi energy scales while both perturbative and non-perturbative results predict that the coupling steeply rises further below the  $\tau$ -scale. Therefore, expecting a perturbative situation with a small coupling does not seem realistic and we choose a conservative maximum interval  $0.5 \lesssim \alpha_s \lesssim 3$  for the effective parameter  $\alpha_s$  that takes into account the combined effects of the strong (non-perturbative) dynamics. Our lower bound is roughly consistent with the value chosen in [22].

$m_{n/p}^*$ : In medium the effective baryon masses  $m_{n/p}^*$  are expected to be somewhat reduced compared to their values in vacuum due to many body effects and since the interactions that cause the dynamic mass generation (as well as chiral symmetry breaking and confinement) are already slightly reduced by both the running of the coupling and charge screening. These three key phenomena of the strongly interacting QCD vacuum are intimately linked, arising from the same non-perturbative dynamics, and therefore it can be expected that in a confined phase the in-medium baryon masses are not dramatically reduced. Correspondingly we consider here a conservative maximum interval of  $0.6 \lesssim m_{n/p}^*/m_{n,p} \lesssim 1$ .

$m_s$ : The fact that the strange quark is much heavier than the light quarks enhances the Urca rate in quark matter. The in-medium strange quark mass  $m_s$  is poorly known due to the impossibility to perform controlled computations at high density. Its lower limit is the current quark mass arising from the Higgs mechanism  $m_{s0} = 93.4_{-3.4}^{+8.6} \text{ MeV}$  (in the  $\overline{\text{MS}}$  scheme at a renormalization scale of  $2 \text{ GeV}$ ) [64]. Dynamical mass generation reduces this value, but since confinement and dynamical mass generation should be intimately linked, in a deconfined phase we expect that the residual mass generation is limited and much smaller than the constituent quark mass values in vacuum. Using a chiral NJL model [65], which lacks confinement and should therefore overestimate the maximum mass of deconfined quarks, as an upper guide, we estimate an upper value of  $200 \text{ MeV}$ . We again consider this as a conservative maximum interval, which gives the  $1\sigma$  range for  $m_s/m_{s0}$  in table I.

$x_p(n_0)$ : The method to absorb the entire dependence of the neutrino emission on the equation of state and

the structure of the star in the single constant  $\tilde{L}$ , eq. (9), requires in the hadronic case in addition merely the proton (or lepton) fraction at saturation density  $x_p(n_0)$ . Due to the chance to perform precise nuclear experiments this value is much better constrained than the composition at high density. We obtained its value from the analysis [66] based on chiral effective theory, which should work well in this regime and yields the  $1\sigma$  interval  $x_p(n_0) = 0.05 \pm 0.002$ .

Symbol	Explanation	Estimated value
$Q_B$	Average heat energy per baryon	$1.545^{\pm 0.19}$ MeV
$M$	Stellar mass	$1.85^{\pm 0.33}$ $M_\odot$
$R$	Stellar radius	$11.8^{\pm 0.9}$ km
$\tilde{L}_{mU}$	Modified Urca luminosity constant	$1.41^{\pm 0.24}$
$\tilde{L}_{dU}$	Direct Urca luminosity constant	$0.99^{\pm 0.07}$
$\tilde{L}_{q\beta}$	Quark beta luminosity constant	$0.70^{\pm 0.048}$
$\alpha_{\text{Urca}}$	Urca off-shell correction factor	$8^{\pm 2.5}$
$\beta_{\text{Urca}}$	Urca short-range correction	$0.83^{\pm 0.22}$
$x_p(n_0)$	Electron fraction at saturation	$0.05^{\pm 0.002}$
$m_n^*/m_n$	In-medium neutron mass fraction	$0.8^{\pm 0.1}$
$m_p^*/m_p$	In-medium proton mass fraction	$0.8^{\pm 0.1}$
$\alpha_s$	Strong coupling constant	$2^{\pm 0.5}$
$m_s^*/m_s$	Strange quark mass fraction	$1.55^{\pm 0.28}$

Table I. Estimated model parameters with  $1\sigma$  uncertainty interval, see the text for details.

## V. STATISTICAL ANALYSIS

To estimate the compatibility of observed sources with different compositional models, we perform a probability analysis. We assume that the various uncertainties are independent and normally distributed. Performing linear error propagation for a general function  $f$  depending on  $n$  independent random variables  $x_i$  with mean values  $\bar{x}_i$  and standard deviations  $\Delta x_i$  the mean value  $\bar{f}$  and standard deviation  $\Delta f$  of the function value is given by [64]

$$\bar{f} = f(\bar{x}_1, \dots, \bar{x}_n)$$

$$\Delta f = \sqrt{\sum_{i=1}^n (\partial_i f(\bar{x}_1, \dots, \bar{x}_n))^2 (\Delta x_i)^2} \quad (24)$$

This expression is justified if the uncertainties are sufficiently small  $\Delta x_i/\bar{x}_i \ll 1$ .

In reality the various input quantities are surely not completely independent. For instance the radius and the mass of the star result from the same solution of the Tolman-Oppenheimer-Volkov equation (depending on the equation of state and the central pressure). However, in practice for neutron stars in a wide range of realistic masses the radius is very insensitive to the

mass, which justifies the assumption in this case. Similarly their poorly constrained probability distributions are generally not perfectly symmetric normal distributions. For instance neutron star masses have an upper and a lower cutoff. Assuming that with a very small probability they can have masses outside of this range we merely overestimate the uncertainty so that our estimates are more conservative than necessary. In addition according to the general version of the central limit theorem, the function  $f$  will in the large  $n$  limit indeed be normally distributed, nearly irrespective of the individual distributions of its various variables. In our case with at most a dozen of dependent variables this limit is surely not reached, but in practice it is found that a normal distribution can be a good approximation already for moderate  $n$ . Therefore, we expect that the assumption of  $f$  being normally distributed with mean value  $\bar{f}$  and standard deviation  $\Delta f$  is a reasonable approximation. Likewise the observational X-ray data (stemming typically from a large number of individual photon counts) can safely be assumed to be approximately normally distributed.

Although we tried to estimate all key uncertainties in the analysis, there are without a doubt further uncertainties that we have not explicitly considered here. This concerns not the least the observational data that can involve various systematic uncertainties and model assumptions. In particular we do not consider errors for the average mass accretion even though there are surely uncertainties involved. In this context it is important to note that the overall error intervals eq. (24) considered here are quite conservative in the sense that we assumed that all these errors add up. The more independent errors there are this becomes more and more unlikely and the various errors should rather partially cancel, which means that our present simplified statistical analysis inherently overestimates the error intervals.

In order to assess the compatibility of a source with a particular model for the cooling within the star, we compute the joint probability of both the data ( $D$ ) and the model ( $M$ ). If they are normally distributed, the two distribution functions  $\pi(x; \bar{x}_M, \Delta x_M)$  and  $\pi(x; \bar{x}_D, \Delta x_D)$  generally intersect at two points  $x_1 < x_2$ . The probability that a given model  $M$  is consistent with a data point  $D$  can be divided up in a sum of the probabilities in the different regions and for independent uncertainties of model and data this gives

$$p(M \cap D) = p(M, x \leq x_1) \times p(D, x \leq x_1)$$

$$+ p(M, x_1 < x \leq x_2) \times p(D, x_1 < x \leq x_2)$$

$$+ p(M, x_2 < x) \times p(D, x_2 < x) \quad (25)$$

For normal distributions the probabilities over the different intervals are given in terms of the cumulative distribution function  $F$

$$\begin{aligned}
p(x \leq x_1) &= F(x_1) \\
p(x_1 < x \leq x_2) &= F(x_2) - F(x_1) \\
p(x_2 < x) &= 1 - F(x_2)
\end{aligned}$$

which in turn can be expressed via the error function

$$F(x; \bar{x}, \Delta x) \equiv \int_{-\infty}^x \pi(x', \bar{x}, \Delta x) dx' = \frac{1}{2} \left( 1 + \operatorname{erf} \left( \frac{x - \bar{x}}{\sqrt{2}\Delta x} \right) \right)$$

In the limit that data and model are clearly separated one can obtain the analytic Gaussian expression

$$p(M \cap D) \xrightarrow[\Delta x_1, \Delta x_2 \ll |\bar{x}_2 - \bar{x}_1|]{1} \sqrt{\frac{2}{\pi}} \frac{1}{\xi} \exp \left( -\frac{\xi^2}{2} \right)$$

in terms of the single parameter

$$\xi \equiv \frac{\bar{x}_2 - \bar{x}_1}{\Delta x_2 + \Delta x_1}$$

which shows that the probability that they are consistent decreases steeply when model and data are sufficiently constrained and far apart (i.e.  $\xi \gg 1$ ).

When it comes to the observational data, in our analysis we consider these statistical expressions to take into account the more easily quantifiable uncertainties in the luminosities in eq. (10), but eventually in the future a more realistic 2D statistical analysis should be performed, that also takes into account the harder quantifiable uncertainties in the average mass accretion rates of these sources.

## VI. RESULTS

Evaluating eq. (10) using the uncertainty ranges in tab. I and performing linear error propagation according to eq. (24) we find asymptotic power law dependencies, where all uncertainties are included in the uncertainty of the prefactors. In case of the fast cooling mechanism these power laws are given for the case that the entire star emits via these direct neutrino processes and they present therefore the maximum possible cooling, while hybrid sources where fast cooling is only possible in a smaller core would be somewhere in between these extreme cases and will be discussed below. These theoretical models are compared to data from various LMXBs taken from table [8, 67] and given in table II.

The results are shown in fig. 1 for a non-accreted envelope and in fig. 2 for a fully-accreted envelope, respectively. As can be seen, despite the substantial uncertainties the curves are in both cases well separated at the  $1\sigma$ -level and do not significantly overlap even at the  $2\sigma$ -level. This is mainly due to the mild parametric dependence on most parameters in eq. (10). Therefore, the

Source	$\langle \dot{M}_{obs} \rangle [M_{\odot}/y]$	$L_q [10^{33} \text{ erg/s}]$	$M [M_{\odot}]$
4U 2129+47	$3.9 \times 10^{-9}$	$1.5^{+3.1}_{-1.2}$	
KS 1731-260	$< 9 \times 10^{-10}$	$0.39^{\pm 0.03}$	$1.61 \pm 0.37$
4U 1608-522	$9.6 \times 10^{-10}$	$5.3^{+4.7}_{-2.9}$	$1.57 \pm 0.30$
1M 1716-315	$< 2.5 \times 10^{-10}$	$1.3^{+1.2}_{-0.7}$	
XTE J1709	$1.8 \times 10^{-10}$	$1.4^{+0.6}_{-0.5}$	
MXB 1659-29	$1.4 \times 10^{-10}$	$0.2^{+0.05}_{-0.11}$	
Cen X-4	$3.8 \times 10^{-11}$	$0.12^{\pm 0.01}$	
4U 1730-22	$< 4.8 \times 10^{-11}$	$2.2^{+2.0}_{-1.1}$	
Aql X-1	$3.2 \times 10^{-10}$	$2.1^{\pm 0.5}$	
NGC 6440 X-1	$6 \times 10^{-11}$	$1.3^{\pm 0.4}$	
IGR J00291	$\sim 2.2 \times 10^{-12}$	$0.19^{+0.06}_{-0.08}$	
HETE J1900.1	$3.9 \times 10^{-11}$	$0.061^{\pm 0.037}$	
Ter5 X-2	$< 1.7 \times 10^{-11}$	$0.7^{\pm 0.1}$	
EXO 0748	$< 4.4 \times 10^{-10}$	$3.8^{\pm 0.2}$	
1RXS J180408	$< 4.6 \times 10^{-11}$	$0.74^{+0.09}_{-0.18}$	
Ter5 X-3	$< 3 \times 10^{-11}$	$1.2^{\pm 0.2}$	

Table II. Accretion observables for transiently accreting LMXBs taken from [8], that have an actual quiescence luminosity measurement (in contrast to only a bound), extended by mass measurements taken from [50] where available.

different models are, even within the various uncertainties, in principle distinguishable.

The minimal cooling of a neutron star is due to slow hadronic modified Urca reactions [68] and in this case photon cooling from the surface dominates at low accretion rates. The transition is around  $10^{-11} M_{\odot}/y$  for a non-accreted envelope and above  $10^{-10} M_{\odot}/y$  for a fully accreted envelope. In the absence of enhanced cooling LMXBs accreting below the lower value inherently cannot probe the interior composition and in the considered data set there are only two such sources (IGR J00291 & XTE J1751) which are well consistent with surface photon emission, while others seem to require enhanced cooling. What is more, for a catalyzed envelope also nearly all hotter sources are well compatible with the minimal modified Urca model. While it is interesting that in the case of a fully accreted envelope fig. 1 photon emission can within uncertainties likewise explain the hotter weakly accreting sources, the strongly accreting sources are in this case even within uncertainties hardly compatible with the minimal modified Urca model and would require a stronger emission mechanism, like pair-breaking emission in nuclear superfluids [69].

In reality the envelope composition varies over time and should be somewhere in between these two extreme cases. Even the average composition could furthermore in principle vary from source to source depending on both the average accretion rate and the number of outbursts. However, as seen from figs. 2 and 1, an intermediate envelope with only limited light element composition (i.e. closer to fig. 1) is within uncertainties consistent with all hotter sources. This might to some extent be surprising

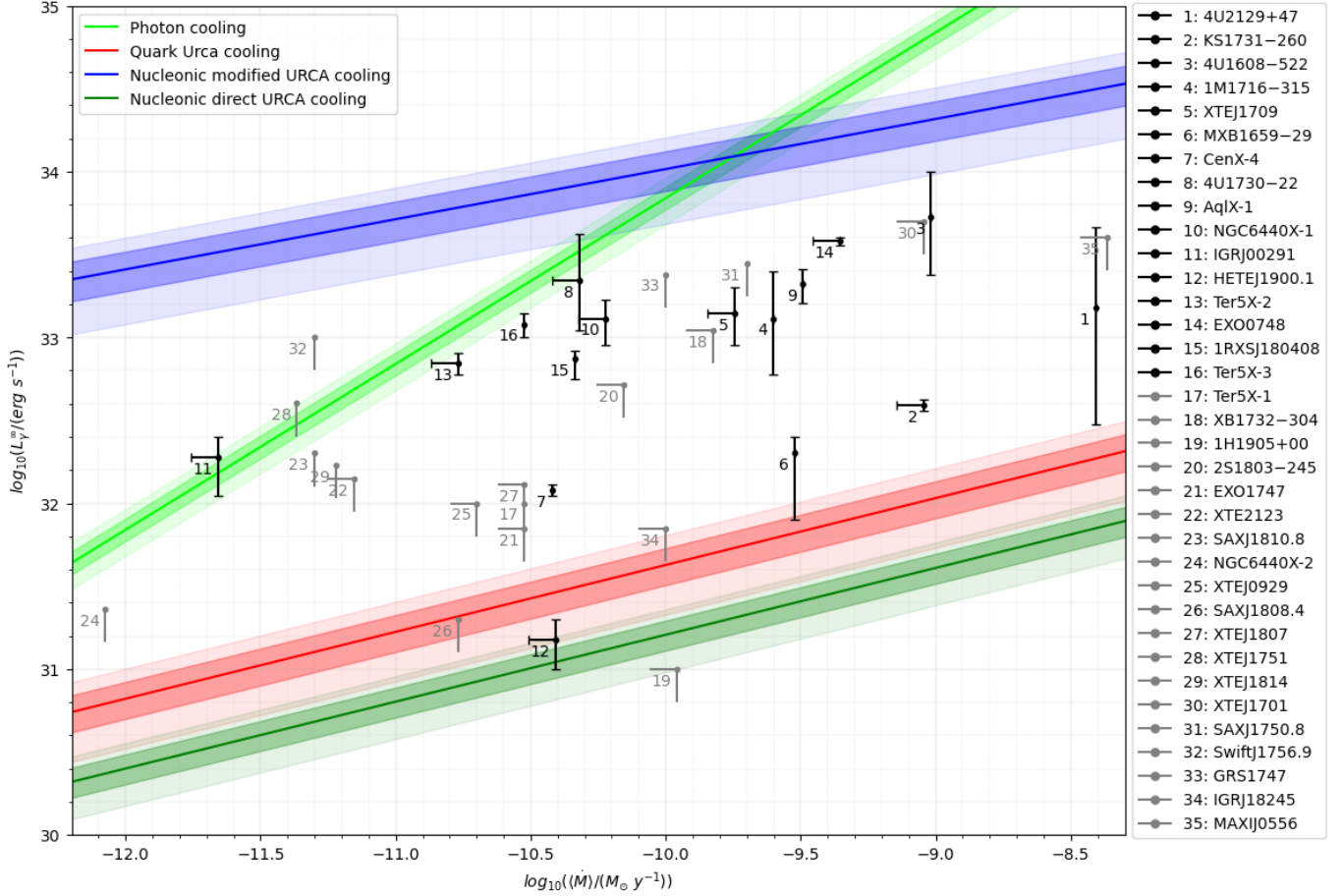


Figure 1. Red-shifted quiescence photon luminosity  $L_\gamma^\infty$  of sources with different dominant emission mechanisms versus averaged accretion rate  $\langle \dot{M} \rangle$  for a fully accreted envelope model [13] compared to LMXB data [8, 67]. Dark and bright colored bands around the theoretical model curves show  $1\sigma$  and  $2\sigma$  errors respectively. The observational errors for the sources in black are  $1\sigma$  intervals, while sources in grey only offer upper bounds.

since higher accretion rates might suggest a larger fraction of light elements. Therefore, this would require an efficient burning of light elements in these sources. Since these sources don't show any bursts or other signs of appreciable accretion in quiescence, a potential explanation might be that when accretion stops the accreted light elements eventually explosively burn without leaving large leftovers and this marks the end of the outburst phase. Such a scenario would not require superfluidity for most sources and taking into account that pair-breaking emission typically only stems from particular density ranges at the boundaries of the superfluid region, this scenario would be far less sensitive to the poorly constrained density dependence of superfluid gaps [70].

Irrespective of the envelope composition, there are several sources that even within the sizable uncertainties significantly deviate from the minimal cooling scenario and clearly require enhanced cooling. In particular, the coldest of these sources seem to require some fast cooling mechanism involving direct Urca reactions. In case of a fully accreted envelope only a maximal core with

hadronic direct Urca [21]—being the most efficient known cooling mechanism [71]—seems to be able to provide the required strength to explain the coldest source 1H 1905+00 [72] while quark Urca emission in a sufficiently large core could potentially explain several of the colder sources (SAX 1808.4, HETE J1900.1, ...).

To quantify the above qualitative statements we consider the probabilities eq. (25) for the compatibility of a particular source with one of the considered models, which are given in tabs. III and IV, respectively. Unfortunately in our statistical analysis we could not consider some of the coldest sources, since they only have an upper luminosity bound and so our simplified Gaussian analysis does not apply (such sources are drawn in grey in figs. 2 and 1). However, there are nonetheless several sources with rather low luminosity measurements, and those with small observational uncertainties are particularly promising. Irrespective of the envelope model the three sources KS1731–260, Cen X-4 and HETE J1900.1 are inconsistent with the minimal cooling model at the  $3.5\sigma$  level, and in case of a fully accreted envelope even

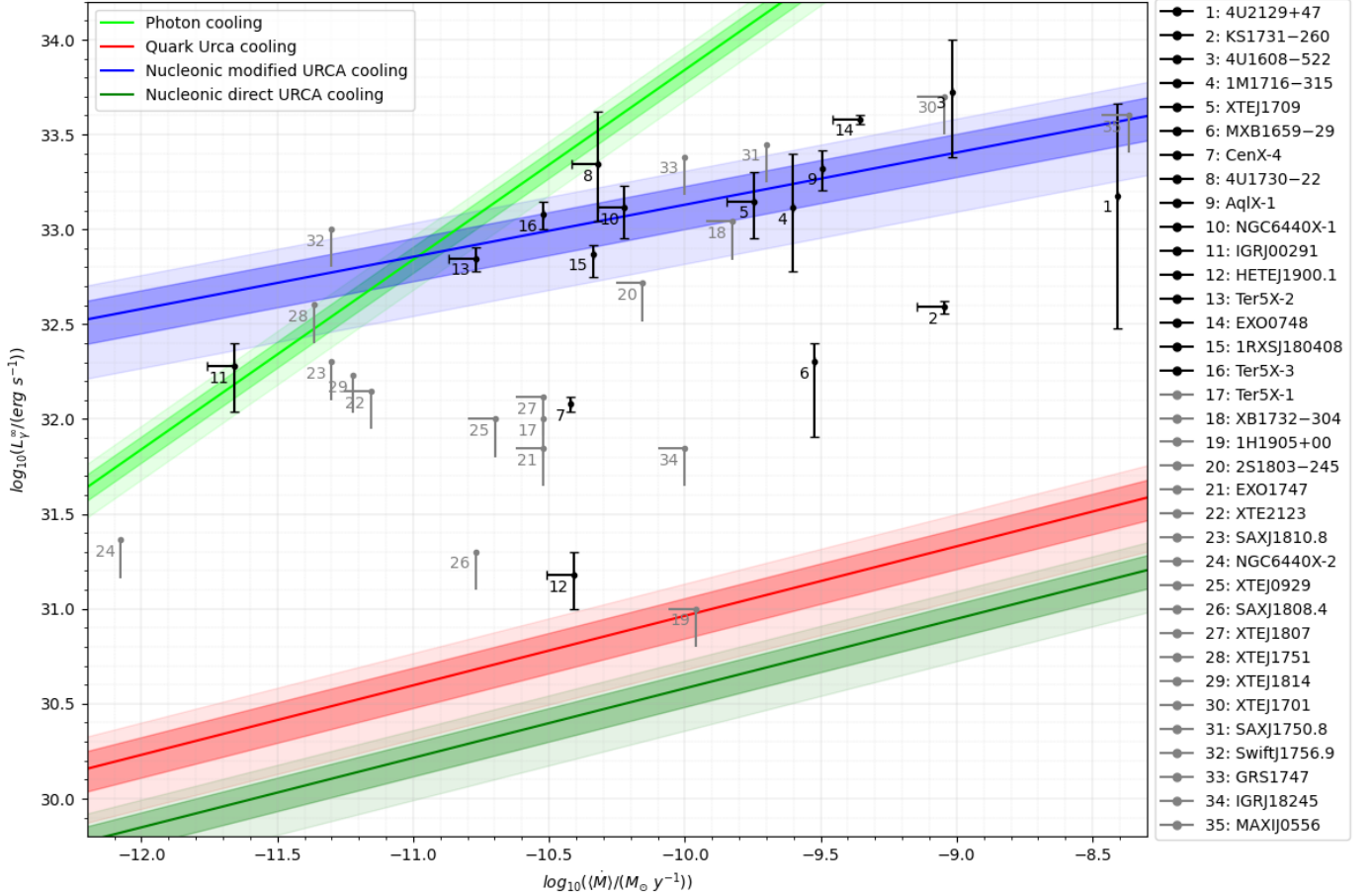


Figure 2. Red-shifted quiescence photon luminosity  $L_\gamma^\infty$  of sources with different dominant emission mechanisms versus averaged accretion rate  $\langle \dot{M} \rangle$  for a fully-catalyzed (non-accreted) iron envelope model [19] compared to LMXB data [8, 67]. Dark and bright colored bands around the theoretical model curves show  $1\sigma$  and  $2\sigma$  errors respectively. The observational errors for the sources in black are  $1\sigma$  intervals, while sources in grey only offer upper bounds.

at the  $4\sigma$  level. In addition MXB 1659–29 challenges the minimal model at the  $3\sigma$  level, so that the combined set of all these sources is clearly statistically incompatible with the minimal model. This shows quantitatively that even within the sizable uncertainties enhanced cooling is required to explain the colder sources in the LMXB data set.

Considering now the compatibility of the extended fast cooling mechanisms with the data, although not surprising, there are several of the hotter sources where fast cooling can be clearly ruled out at better than the  $5\sigma$  level. In case of a non-accreted crust, where the hotter sources are well described by modified Urca emission, those that are not, are also not well compatible with either of the extreme fast cooling models. Therefore either some intermediate mechanism [69] (e.g. in superfluids [8]) or a hybrid source with a smaller inner core, either made of quark matter or where hadronic Urca reactions are allowed, would be required to explain these sources, as discussed below. In contrast for a fully accreted crust even the extreme quark matter model [73] is marginally consist-

ent with some of the colder sources. In this context it is important to note that the quark Urca emissivity can be enhanced by non-Fermi liquid effects [39] stemming from unscreened interactions in dense quark matter. These introduce logarithmic temperature dependences (eq. (6)) that can be sizable at very low temperature, but are expected to be mild for these heated sources. Including these effects in the future will require a computationally somewhat more elaborate analysis.

When it comes to the actual compatibility of a data point with a given model the larger probabilities in the tables are less conclusive. The reason for this is that even if model and data agree well with each other the computed probability can depend strongly on the uncertainties. For instance, for a data point with a very small uncertainty and a model centered at exactly the same point the computed probability is the smaller the larger the model uncertainties are, so that merely our ignorance, or aspiration to estimate a conservative interval, can make the probability small. In contrast, if model and data are far apart a larger uncertainty actually increases

Source	$p_\gamma$	$p_{\text{mU}}$	$p_{\text{dU}}$	$p_{\text{qU}}$	$M_{\text{c,dU}}/M$	$M_{\text{c,qU}}/M$
4U 2129+47	-	$8.5 \times 10^{-3}$	$1.2 \times 10^{-2}$	$3.4 \times 10^{-2}$	$5.1 \times 10^{-4}$	$5.9 \times 10^{-3}$
KS 1731-260*	-	$2.8 \times 10^{-5}$	-	$2.8 \times 10^{-7}$	$3.3 \times 10^{-3}$	$3.8 \times 10^{-2}$
4U 1608-522	-	$1.3 \times 10^{-1}$	$2.9 \times 10^{-3}$	$8.7 \times 10^{-3}$	$5.4 \times 10^{-6}$	$6.3 \times 10^{-5}$
1M 1716-315*	-	$9.6 \times 10^{-3}$	$6.5 \times 10^{-3}$	$2.0 \times 10^{-2}$	$4.7 \times 10^{-5}$	$5.4 \times 10^{-4}$
XTE J1709	-	$3.9 \times 10^{-3}$	$1.6 \times 10^{-3}$	$5.4 \times 10^{-3}$	$2.8 \times 10^{-5}$	$3.2 \times 10^{-4}$
MXB 1659-29	-	$7.8 \times 10^{-5}$	$4.3 \times 10^{-4}$	$1.2 \times 10^{-2}$	$2.7 \times 10^{-3}$	$3.1 \times 10^{-2}$
Cen X-4	-	$2.4 \times 10^{-5}$	-	$1.1 \times 10^{-7}$	$2.6 \times 10^{-3}$	$3.0 \times 10^{-2}$
4U 1730-22*	$6 \times 10^{-1}$	-	$2.1 \times 10^{-3}$	$6.4 \times 10^{-3}$	$2.4 \times 10^{-6}$	$2.8 \times 10^{-5}$
Aql X-1	-	$3.1 \times 10^{-3}$	$8.2 \times 10^{-6}$	$3.7 \times 10^{-5}$	$1.8 \times 10^{-5}$	$2.1 \times 10^{-4}$
NGC 6440 X-1	$4.2 \times 10^{-2}$	-	$1.4 \times 10^{-4}$	$5.1 \times 10^{-4}$	$1.1 \times 10^{-5}$	$1.3 \times 10^{-4}$
IGR J00291	$1.3 \times 10^{-1}$	-	$3.3 \times 10^{-4}$	$1.4 \times 10^{-3}$	$4.8 \times 10^{-5}$	$5.6 \times 10^{-4}$
HETEJ1900.1	-	$1.0 \times 10^{-5}$	$3.9 \times 10^{-1}$	$2.2 \times 10^{-1}$	$4.6 \times 10^{-1}$	-
Ter5 X-2*	$1.8 \times 10^{-1}$	-	$4.3 \times 10^{-12}$	$6.5 \times 10^{-11}$	$1.5 \times 10^{-5}$	$1.7 \times 10^{-4}$
EXO 0748*	-	$2.6 \times 10^{-3}$	-	-	$5.7 \times 10^{-6}$	$6.6 \times 10^{-5}$
1RXS J180408*	$1.6 \times 10^{-2}$	-	$1.7 \times 10^{-15}$	$2.8 \times 10^{-13}$	$3.5 \times 10^{-5}$	$4.0 \times 10^{-4}$
Ter5 X-3*	$2.6 \times 10^{-1}$	-	$1.2 \times 10^{-9}$	$7.0 \times 10^{-9}$	$6.8 \times 10^{-6}$	$7.9 \times 10^{-5}$

Table III. Probabilities for the compatibility of different core cooling models ( $\gamma$ : photon emission, mU: nucleonic modified Urca, dU: nucleonic direct Urca, qU: quark Urca) with the various sources as well as hybrid star core mass fractions for a fully-accreted light element envelope [13]. Sources marked by a star only have an upper bound on the mass accretion rate.

Source	$p_\gamma$	$p_{\text{mU}}$	$p_{\text{dU}}$	$p_{\text{qU}}$	$M_{\text{c,dU}}/M$	$M_{\text{c,qU}}/M$
4U 2129+47	-	$3.3 \times 10^{-1}$	$2.6 \times 10^{-3}$	$7.0 \times 10^{-3}$	$3.1 \times 10^{-6}$	$3.4 \times 10^{-5}$
KS 1731-260*	-	$7.6 \times 10^{-4}$	-	-	$2.9 \times 10^{-5}$	$3.2 \times 10^{-4}$
4U 1608-522	-	$2.0 \times 10^{-1}$	$6.7 \times 10^{-4}$	$1.8 \times 10^{-3}$	-	-
1M 1716-315*	-	$4.0 \times 10^{-1}$	$1.6 \times 10^{-3}$	$4.3 \times 10^{-3}$	$2.0 \times 10^{-7}$	$2.2 \times 10^{-6}$
XTE J1709	-	$5.0 \times 10^{-1}$	$3.7 \times 10^{-4}$	$1.0 \times 10^{-3}$	$6.4 \times 10^{-8}$	$7.1 \times 10^{-7}$
MXB 1659-29	-	$2.0 \times 10^{-3}$	$3.3 \times 10^{-5}$	$1.5 \times 10^{-4}$	$2.8 \times 10^{-5}$	$3.1 \times 10^{-4}$
Cen X-4	-	$3.6 \times 10^{-4}$	-	-	$3.1 \times 10^{-5}$	$3.4 \times 10^{-4}$
4U 1730-22*	-	$2.1 \times 10^{-1}$	$5.5 \times 10^{-4}$	$1.5 \times 10^{-3}$	-	-
Aql X-1	-	$4.8 \times 10^{-1}$	$1.6 \times 10^{-6}$	$4.8 \times 10^{-6}$	-	-
NGC 6440 X-1	-	$5.2 \times 10^{-1}$	$3.3 \times 10^{-5}$	$9.3 \times 10^{-5}$	-	-
IGR J00291	$1.3 \times 10^{-1}$	-	$8.3 \times 10^{-5}$	$2.4 \times 10^{-4}$	$4.9 \times 10^{-7}$	$5.4 \times 10^{-6}$
HETE J1900.1	-	$4.5 \times 10^{-5}$	$1.5 \times 10^{-2}$	$1.5 \times 10^{-1}$	$9.2 \times 10^{-3}$	$1.0 \times 10^{-1}$
Ter5 X-2*	-	$4.3 \times 10^{-1}$	$6.6 \times 10^{-13}$	$2.4 \times 10^{-12}$	$5.1 \times 10^{-8}$	$5.7 \times 10^{-7}$
EXO 0748*	-	$1.2 \times 10^{-2}$	-	-	-	-
1RXS J180408*	-	$2.4 \times 10^{-1}$	$1.1 \times 10^{-16}$	$6.1 \times 10^{-16}$	$2.0 \times 10^{-7}$	$2.2 \times 10^{-6}$
Ter5 X-3*	-	$4.3 \times 10^{-1}$	$2.3 \times 10^{-10}$	$7.1 \times 10^{-10}$	-	-

Table IV. Probabilities for the compatibility of different core cooling models with the various sources as well as hybrid star core mass fractions for a catalyzed iron envelope [19]. Sources marked by a star only have an upper bound on the mass accretion rate.

the probability that they are compatible. Therefore, if we nonetheless find a small probability for the compatibility this represents an upper bound even if we overestimated the uncertainties. Correspondingly, sufficiently large probabilities in the tables merely qualitatively signal compatibility, but cannot really quantify it, whereas small probabilities indeed quantify the incompatibility.

Finally we estimate the sizes of the required fast cooling cores to explain the observational sources with either of the fast cooling models. Using eq. (12), yields

the mass fractions given in tables III and IV, where our present analysis does not allow us to consistently consider the uncertainties in the analysis. As can be seen for many of the hotter sources the required cores are small for quark matter and even significantly smaller for hadronic Urca cooling. Yet, for several of the colder sources the required hybrid star cores are larger, and when taking into account the uncertainties in the analysis it can be expected that even larger quark cores than in tables III and IV are compatible with the data. Furthermore if

quark matter is color superconducting [48] the emissivity is reduced—e.g. in the classic 2SC phase by an effective reduction factor 5/9 reflecting the ungapped quark flavors—bringing such a model even closer to the data.

## VII. CONCLUSION

In this work we assessed the deep crustal heating scenario, taking into account the various micro- and astrophysical uncertainties in the analysis. We find that despite the numerous, and in several cases sizable, uncertainties, deep crustal heating has the potential to probe the properties of the star’s interior and discriminate different compositional scenarios. This is not the least due to the fortunate fact that the relation between the astrophysical observables eq. (10) is, similarly to the case of r-mode damping [33, 38], rather insensitive to key uncertainties in the analysis.

As discussed, the composition of the crust has a strong influence on the cooling. We find that a mostly catalyzed envelope can consistently explain all the hotter sources via standard modified Urca emission, while assuming a strongly accreted envelope would require enhanced cooling e.g. due to superfluidity. Observed sources should be in between the studied extreme cases. This would mean that if modified Urca is indeed the dominant mechanism in these sources, the most outer layers of the crust responsible for its heat insulation should catalyze quickly so that only little light elements remain during most of the quiescence period. In this context it is interesting that the relaxation of the crust observed by the time-dependent cooling behavior during quiescence [74] can potentially directly probe the composition of the crust. This would eliminate this key uncertainty and thereby enable a more rigorous analysis to probe the core composition.

However, our analysis also shows that even when taking into account these various uncertainties several colder sources clearly statistically challenge the minimal scenario where LMXBs merely cool via slow modified Urca reactions with an emissivity  $\sim (T/p_F)^8$ . Therefore, it highlights the well known conclusion that there is very likely not a single mechanism that can explain all observed sources [6–8, 67], pointing to some sort of extended composition beyond minimal  $npe\mu$ -matter.

In this work we considered selected extended models of the interior composition of neutron stars, featuring fast neutrino emission processes  $\sim (T/p_F)^6$ , namely hadronic direct Urca and quark Urca. In particular we considered here the extreme case that the entire star emits via a single mechanism and find that such a strong cooling is statistically inconsistent with all but the coldest sources. Yet, if fast cooling is only realized in an inner core whose size depends on details of the equation of state this naturally reduces the emissivity. There are also intermediate processes  $\sim (T/p_F)^7$  [40], e.g. from pair-breaking and formation in superfluids or meson condensates, that

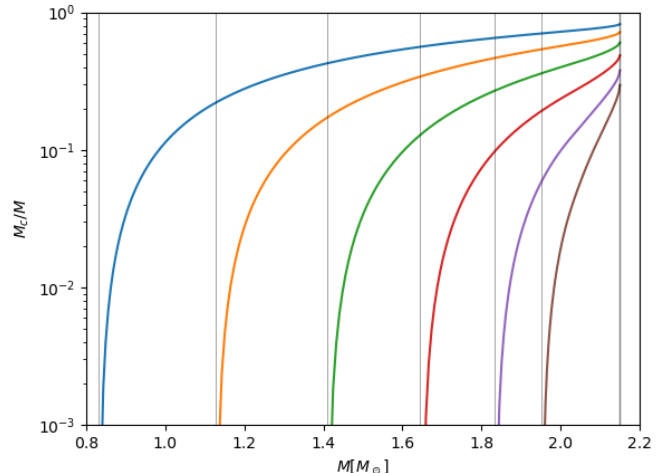


Figure 3. Mass ratio  $M_c/M$  of an inner core (with enhanced neutrino emission) for various exemplary values of the transition density as a function of the mass  $M$  of the star. Thin vertical lines mark the corresponding critical masses where an inner core appears and the thick vertical line marks the maximum mass configuration.

have the potential to explain the data and it would be interesting to perform an analogous statistical analysis for such compositions in the future. When it comes to superfluidity [70], generically only part of the star can be superfluid and it depends strongly on the density dependence of the superfluid gap. Moreover, there are various other exotic phases of matter that could be compared to the data to see if these are consistent with a subset of the sources.

Taking into account that a minimal hadronic ( $npe\mu$ ) composition can feature at the same time both the slowest [20] and nearly the fastest known cooling processes [43] and that the cooling luminosity can depending on the not directly observable size of the direct Urca core in principle even take any intermediate value, it might seem that it is inherently impossible to detect any exotic composition through its cooling behavior in transiently accreting neutron stars. And even more so, when considering that the probably most interesting exotic composition—deconfined quark matter—likewise can be based on the size of the quark core yield in principle any intermediate cooling behavior. However, our results here show that the situation is actually much more promising. To see this recall that according to figs. 1 and 2 (maximal) quark Urca and hadronic direct Urca cooling are, even within the sizable uncertainties, clearly distinguishable. The quark matter and hadronic Urca emissivities are many orders of magnitude larger than modified Urca. Using eq. (12), this would require dramatically small cores to explain these sources, as seen in tables III and IV. However, as seen in fig. 3, a very small quark core would require a star mass just above the critical value for a given equation

of state where an inner core arises. Since the masses stem from the accretion history and should be continuously distributed, such a clustering of several sources in a very narrow interval would be extremely unlikely and therefore generally only sufficiently large cores are expected. Correspondingly, with sufficient data such a scenario could be statistically challenged. Moreover, with additional mass measurements for these sources such a scenario can be directly checked since the source mass would have to monotonously increase from sources with large to small photon emissivity (ranging from slow to fast neutrino cooling).

Interestingly, there are already mass estimates for the two sources KS 1731–260 and 4U 1608–522 [50] which might have similar mass accretion rates (the value for the former source being only an upper bound) and also have very similar mass estimates. Yet, they have markedly different quiescence luminosities that differ by more than an order of magnitude, so that 4U 1608–522 is consistent with modified Urca cooling while KS 1731–260 could based on the envelope composition be compatible with being a hybrid star. The colder of them KS 1731–260 indeed seems to have a slightly larger mass (although this is so far not significant within the large uncertainties), so that if this mass ordering persists in more precise mea-

surements and quark matter would indeed be the reason for its low luminosity, this could point to a critical mass where quark matter arises around  $1.6 M_{\odot}$ .

Taking into account that, even within uncertainties, hadronic and quark phases of dense matter can show a markedly different fast cooling behavior, there is a realistic chance that nucleonic and exotic phases can be discriminated via a careful statistical analysis based on a sufficiently large and precise astrophysical dataset. Such a discrimination of different compositional scenarios of the neutron star interior is even more promising considering other observed dynamic processes that can probe the cooling behavior or even other material properties. A prime example is the damping of r-modes both in LMXBs and other sources, which also probes the viscous dissipation and thereby imposes independent constraints that can distinguish different phases of matter [32, 33, 38].

## ACKNOWLEDGMENTS

This work was supported by the Turkish Research Council (TÜBİTAK) via project 117F312.

- 
- [1] Q. Z. Liu, J. van Paradijs, and E. P. J. v. den Heuvel, *Astron. Astrophys.* **469**, 807 (2007), arXiv:0707.0544 [astro-ph].
  - [2] S. L. Shapiro and S. A. Teukolsky, *Black holes, white dwarfs and neutron stars. The physics of compact objects* (1983).
  - [3] P. Haensel, A. Y. Potekhin, and D. G. Yakovlev, *Neutron Stars 1* (Springer, 2007).
  - [4] M. A. Alpar, A. F. Cheng, M. A. Ruderman, and J. Shaham, *Nature (London)* **300**, 728 (1982).
  - [5] A. Y. Potekhin, *Physics-Uspeski* **53**, 1235 (2010).
  - [6] D. G. Yakovlev and C. J. Pethick, *Ann. Rev. Astron. Astrophys.* **42**, 169 (2004).
  - [7] R. Wijnands, N. Degenaar, and D. Page, *J. Astrophys. Astron.* **38**, 49 (2017).
  - [8] A. Y. Potekhin, A. I. Chugunov, and G. Chabrier, *Astronomy & Astrophysics* **629**, A88 (2019).
  - [9] N. Chamel and P. Haensel, *Living Reviews in relativity* **11**, 1 (2008).
  - [10] M. Beznogov, A. Potekhin, and D. Yakovlev, *Physics Reports* **919**, 1 (2021).
  - [11] M. V. Beznogov, A. Y. Potekhin, M. Fortin, P. Haensel, J. L. Zdunik, and D. G. Yakovlev, *Journal of Physics: Conference Series* **932**, 012046 (2017).
  - [12] P. Haensel and J. L. Zdunik, *Astron. Astrophys.* **227**, 431 (1990).
  - [13] A. Y. Potekhin, G. Chabrier, and D. G. Yakovlev, “Internal temperatures and cooling of neutron stars with accreted envelopes,” (1997).
  - [14] P. Haensel and J. L. Zdunik, *Astronomy & Astrophysics* **404**, L33 (2003).
  - [15] P. Haensel and J. L. Zdunik, *Astronomy & Astrophysics* **480**, 459 (2008).
  - [16] A. F. Fantina, J. L. Zdunik, N. Chamel, J. M. Pearson, P. Haensel, and S. Gorieli, *Astron. Astrophys.* **620**, A105 (2018), arXiv:1806.03861 [astro-ph.HE].
  - [17] E. F. Brown, L. Bildsten, and R. E. Rutledge, *The Astrophysical Journal* **504**, L95 (1998).
  - [18] E. F. Brown, L. Bildsten, and P. Chang, *Astrophys. J.* **574**, 920 (2002), arXiv:astro-ph/0204102.
  - [19] E. H. Gudmundsson, C. J. Pethick, and R. I. Epstein, *Astrophysical Journal* **259**, L19 (1982).
  - [20] B. L. Friman and O. V. Maxwell, *Astrophysical Journal*, Part 1, vol. 232, Sept. 1, 1979, p. 541-557. **232**, 541 (1979).
  - [21] J. M. Lattimer, K. A. van Riper, M. Prakash, and M. Prakash, **425**, 802 (1994).
  - [22] N. Iwamoto, *Physical Review Letters* **44**, 1637 (1980).
  - [23] K. S. Thorne, in *High Energy Astrophysics, Volume 3*, Vol. 3, edited by C. Dewitt, E. Schatzman, and P. Véron (1967) p. V.
  - [24] K. S. Thorne, *Astrophys. J.* **212**, 825 (1977).
  - [25] J. R. Oppenheimer and G. M. Volkoff, *Physical Review* **55**, 374 (1939).
  - [26] R. C. Tolman, *Physical Review* **55**, 364 (1939).
  - [27] D. G. Yakovlev and C. Pethick, *Annu. Rev. Astron. Astrophys.* **42**, 169 (2004).
  - [28] G. Glen and P. Sutherland, *Astrophysical Journal*, Part 1, vol. 239, July 15, 1980, p. 671-684. Research supported by the Natural Sciences and Engineering Research Council of Canada. **239**, 671 (1980).
  - [29] D. G. Yakovlev, K. P. Levenfish, and P. Haensel, *Astron. Astrophys.* **407**, 265 (2003), arXiv:astro-ph/0209027.
  - [30] A. Y. Potekhin, D. A. Zyuzin, D. G. Yakovlev, M. V.

- Beznogov, and Y. A. Shibarov, *Monthly Notices of the Royal Astronomical Society* **496**, 5052 (2020).
- [31] A. Reisenegger, *Astrophys. J.* **442**, 749 (1995), arXiv:astro-ph/9410035.
- [32] N. Andersson and K. D. Kokkotas, *Int. J. Mod. Phys. D* **10**, 381 (2001), arXiv:gr-qc/0010102.
- [33] M. Alford, S. Mahmoodifar, and K. Schwenzer, *Phys.Rev.* **D85**, 024007 (2012), arXiv:1012.4883 [astro-ph.HE].
- [34] T. Boztepe, E. Göğüs, T. Güver, and K. Schwenzer, *Mon. Not. Roy. Astron. Soc.* **498**, 2734 (2020), arXiv:1910.04448 [astro-ph.HE].
- [35] P. Haensel and J. Zdunik, *Astronomy & Astrophysics* **480**, 459 (2008).
- [36] The heating is localized at the boundary where the heat balance can be established. Correspondingly the heating power at infinity is a mere definition arising when rewriting the heat balance equation in terms of luminosities at infinity. The linear dependence on the metric factor compared to the luminosities below that are quadratic in it, stems from the fact that the energy gained when matter is falling into the gravitational potential well does not contribute to deep crustal heating but is directly radiated off at the surface.
- [37] A. Y. Potekhin, G. Chabrier, and D. G. Yakovlev, *Astron. Astrophys.* **323**, 415 (1997), arXiv:astro-ph/9706148.
- [38] M. G. Alford and K. Schwenzer, *Phys.Rev.Lett.* **113**, 251102 (2014), arXiv:1310.3524 [astro-ph.HE].
- [39] T. Schafer and K. Schwenzer, *Phys. Rev.* **D70**, 114037 (2004), arXiv:astro-ph/0410395.
- [40] D. G. Yakovlev, A. D. Kaminker, O. Y. Gnedin, and P. Haensel, *Phys. Rept.* **354**, 1 (2001), arXiv:astro-ph/0012122.
- [41] Even though such a configuration could in principle be stable in the absence of gravity, it would require gravity to form it.
- [42] A. Akmal, V. R. Pandharipande, and D. G. Ravenhall, *Phys. Rev.* **C58**, 1804 (1998), arXiv:nucl-th/9804027.
- [43] J. M. Lattimer, C. Pethick, M. Prakash, and P. Haensel, *Physical review letters* **66**, 2701 (1991).
- [44] P. S. Shternin, M. Baldo, and P. Haensel, *Phys. Lett. B* **786**, 28 (2018), arXiv:1807.06569 [astro-ph.HE].
- [45] N. Brambilla *et al.*, *Eur. Phys. J. C* **74**, 2981 (2014), arXiv:1404.3723 [hep-ph].
- [46] M. G. Alford, S. Reddy, and K. Schwenzer, *Phys. Rev. Lett.* **108**, 111102 (2012), arXiv:1110.6213 [nucl-th].
- [47] A. Deur, S. J. Brodsky, and C. D. Roberts, *Prog. Part. Nucl. Phys.* **134**, 104081 (2024), arXiv:2303.00723 [hep-ph].
- [48] M. G. Alford, A. Schmitt, K. Rajagopal, and T. Schafer, *Rev. Mod. Phys.* **80**, 1455 (2008), arXiv:0709.4635 [hep-ph].
- [49] J. G. Martinez, K. Stovall, P. C. C. Freire, J. S. Deneva, F. A. Jenet, M. A. McLaughlin, M. Bagchi, S. D. Bates, and A. Ridolfi, *The Astrophysical Journal* **812**, 143 (2015).
- [50] F. Özel and P. Freire, *Ann. Rev. Astron. Astrophys.* **54**, 401 (2016), arXiv:1603.02698 [astro-ph.HE].
- [51] P. Demorest, T. Pennucci, S. Ransom, M. Roberts, and J. Hessels, *Nature* **467**, 1081 (2010), arXiv:1010.5788 [astro-ph.HE].
- [52] H. T. Cromartie *et al.* (NANOGrav), *Nature Astron.* **4**, 72 (2019), arXiv:1904.06759 [astro-ph.HE].
- [53] R. W. Romani, D. Kandel, A. V. Filippenko, T. G. Brink, and W. Zheng, *Astrophys. J. Lett.* **934**, L17 (2022), arXiv:2207.05124 [astro-ph.HE].
- [54] L. Rezzolla, E. R. Most, and L. R. Weih, *Astrophys. J. Lett.* **852**, L25 (2018), arXiv:1711.00314 [astro-ph.HE].
- [55] M. Ruiz, S. L. Shapiro, and A. Tsokaros, *Phys. Rev. D* **97**, 021501 (2018), arXiv:1711.00473 [astro-ph.HE].
- [56] J. M. Lattimer and A. W. Steiner, *Astrophys. J.* **784**, 123 (2014), arXiv:1305.3242 [astro-ph.HE].
- [57] F. Özel, D. Psaltis, T. Guver, G. Baym, C. Heinke, and S. Guillot, *Astrophys. J.* **820**, 28 (2016), arXiv:1505.05155 [astro-ph.HE].
- [58] M. C. Miller *et al.*, *Astrophys. J. Lett.* **887**, L24 (2019), arXiv:1912.05705 [astro-ph.HE].
- [59] M. C. Miller *et al.*, *Astrophys. J. Lett.* **918**, L28 (2021), arXiv:2105.06979 [astro-ph.HE].
- [60] M. G. Alford, S. Han, and M. Prakash, *Phys. Rev. D* **88**, 083013 (2013), arXiv:1302.4732 [astro-ph.SR].
- [61] A. F. Fantina, J. L. Zdunik, N. Chamel, J. M. Pearson, L. Suleiman, and S. Goriely, *Astron. Astrophys.* **665**, A74 (2022), arXiv:2209.11457 [astro-ph.HE].
- [62] A. W. Steiner, *Phys. Rev. C* **85**, 055804 (2012), arXiv:1202.3378 [nucl-th].
- [63] The integrals that define  $\alpha_{\text{Urca}}$  in this improved approximation evaluate to simple analytic expressions describing its mild density dependence away from threshold, but it eventually increases dramatically over a narrow interval towards the 6-7 orders of magnitude direct Urca emissivity. In this approximation  $\alpha_{\text{Urca}}$  even formally diverges at the Urca threshold, but this can easily be regulated to obtain a realistic behavior.
- [64] R. L. Workman *et al.* (Particle Data Group), *PTEP* **2022**, 083C01 (2022).
- [65] M. Buballa, *Physics Reports* **407**, 205 (2005).
- [66] E. S. Fraga, R. da Mata, and J. Schaffner-Bielich, *Physical Review D* **108**, 116003 (2023).
- [67] A. Y. Potekhin, M. E. Gusakov, and A. I. Chugunov, *Mon. Not. Roy. Astron. Soc.* **522**, 4830 (2023), arXiv:2303.08716 [astro-ph.HE].
- [68] There are slower processes like bremsstrahlung [69] that can be present in addition, but modified Urca should be realized unless large parts of the star are superfluid and superconducting, which is not expected. Therefore, it is rather the fastest of the slow processes that are expected for a minimal ( $npe\mu$ ) neutron star composition, while various enhanced processes are only present under certain conditions.
- [69] D. G. Yakovlev, A. D. Kaminker, O. Y. Gnedin, and P. Haensel, *Phys. Rept.* **354**, 1 (2001).
- [70] A. Sedrakian and J. W. Clark, *Eur. Phys. J. A* **55**, 167 (2019), arXiv:1802.00017 [nucl-th].
- [71] Hyperonic direct Urca could have a slightly higher emissivity than purely non-strange reactions.[6].
- [72] Assuming the current bound for this faint source is not too low as was the case for SAX 1808.4 and which had to be corrected upwards quite substantially over time [8, 75].
- [73] In the case of quark matter such a strange star with a maximal quark core would likely require the strange matter hypothesis [76].
- [74] E. F. Brown and A. Cumming, *Astrophys. J.* **698**, 1020 (2009), arXiv:0901.3115 [astro-ph.SR].
- [75] S. Han, A. W. Steiner, *et al.*, *Physical Review C* **96**, 35802 (2017).
- [76] E. Witten, *Phys. Rev.* **D30**, 272 (1984).